JOURNAL OF GEOPHYSICAL RESEARCH, VOL. 115, A01214, doi:10.1029/2009JA014321, 2010

On the causes of plasmaspheric rotation variability: IMAGE EUV observations

David A. Galvan,[1,2] Mark B. Moldwin,[1,3] Bill R. Sandel,[4] and Geoff Crowley[5]

Received 31 March 2009; revised 15 August 2009; accepted 23 September 2009; published 29 January 2010.

[1] IMAGE EUV observations demonstrate that the plasmasphere usually does not corotate as assumed in simple convection models, even at low L shells. We carry out a statistical survey of plasmaspheric rotation rates over several months of IMAGE EUV data in 2001, using two different measurement techniques. We test the prevailing hypothesis, that subcorotation is due to enhanced auroral zone Joule heating driving equatorward thermospheric winds, by testing for correlation of rotation rates with several geomagnetic indices. Azimuthal features such as "notches" are tracked in local time over a single pass of the IMAGE satellite, both visually and using an automated cross-correlation routine. Each technique provides an estimate of the plasmasphere's rotation rate. We find a weak correlation between rotation rate and *Dst*, *Kp*, *AE*, the midnight boundary index (MBI), and Joule heating estimates from assimilative mapping of ionospheric electrodynamics (AMIE) at $L = 2.5$, but not at $L = 3.5$. In general, lower rotation rates correspond to higher auroral and geomagnetic activity. We also make the first direct observation of plasmaspheric superrotation. The plasmaspheric rotation rate is found to be highly variable on multiday timescales, but the typical state of the plasmasphere is subcorotation, with inferred mean values ranging from 88% to 95% of corotation, depending on L shell. In addition, a statistical analysis shows that rotation rates near dusk are generally lower than those at dawn, suggesting that local time and magnetospheric convection contribute to the variation in rotation rate as well. We conclude that the cause of variability in plasmaspheric rotation rate is a combination of storm phase, local-time-dependent convection, and westward ionospheric drift.

Citation: Galvan, D. A., M. B. Moldwin, B. R. Sandel, and G. Crowley (2010), On the causes of plasmaspheric rotation variability: IMAGE EUV observations, *J. Geophys. Res.*, *115*, A01214, doi:10.1029/2009JA014321.

1. Introduction

[2] Planets with both an atmosphere and a global magnetic field display the phenomenon of corotation, where magnetospheric plasma rotates with roughly the same angular velocity as the planet below. This begins through a viscous interaction between the planetary surface and the neutral atmosphere, and momentum is transferred to the ionosphere via collisional friction. Once the ionospheric plasma is rotating with the planet, it generates a corotation electric field which, under the assumption of an infinitely conducting plasma (the "frozen-in flux" condition), is described by

$$E = -(w \times r) \times B, \tag{1}$$

where w is the angular rotation rate of the planet, B is the magnetic field, and r is the distance from the center of the planet. This corotation electric field is projected along magnetic field lines out into space and serves to enforce the corotation of low-energy plasma outside the atmosphere [*Mozer*, 1970, 1973; *Hill*, 1979]. At Earth, this body of corotating plasma is known as the plasmasphere. Bodies without significant neutral atmospheres may still be able to maintain a corotation electric field if the surface conductivity is high enough, and this may be an important phenomenon for neutron stars [*Gold*, 1968; *Romanova et al.*, 2002]. Mercury, with a much weaker magnetic field than the Earth and an exosphere composed of sodium sputtered from the surface, likely does not have a strong corotation electric field. Its small magnetosphere is likely dominated by convection [*Slavin et al.*, 2008].

[3] Departures from perfect corotation of magnetospheric plasma can be caused by a variety of mechanisms, including external forces such as magnetospheric convection [*Nishida*,

[1]Institute of Geophysics and Planetary Physics, Department of Earth and Space Sciences, University of California, Los Angeles, California, USA.
[2]Now at Jet Propulsion Laboratory, California Institute of Technology, Pasadena, California, USA.
[3]Now at Department of Atmospheric, Oceanic and Space Sciences, University of Michigan, Ann Arbor, Michigan, USA.
[4]Lunar and Planetary Laboratory, University of Arizona, Tucson, Arizona, USA.
[5]Atmospheric and Space Technology Research Associates, San Antonio, Texas, USA.

0148-0227/10/2009JA014321$09.00

1966; *Brice*, 1967], magnetospheric mass loading due to charge exchange at volatile moons (as is the case at Saturn [*Tokar et al.*, 2006] and Jupiter [e.g., *Pontius and Hill*, 1982; *Brown*, 1983; *Brown*, 1994; *Kronberg et al.*, 2007]), or an inertial lag caused by the outward transport of plasma [*Hill*, 1979]. Also, the degree to which the ionosphere couples with the magnetosphere to produce an effective corotation electric field will depend on ionospheric conductivity gradients in local time and latitude [e.g., *Senior and Blanc*, 1984]. The transmission of the ionospheric electric field to the magnetosphere is carried out by Alfvén waves, which travel along the field lines at finite speeds that depend on the local magnetic field and plasma density ($v_a = B/\sqrt{\mu\rho}$, where B is the magnetic field strength, μ is the permeability, and ρ is the plasma mass density). A change in rotation rate in the ionosphere would result in a change in the ionospheric corotation electric field, which would then propagate out into the magnetosphere at roughly the Alfvén speed. Thus, there is an inherent lag in the synchronization of the ionospheric and magnetospheric corotation electric fields, which should increase with L because of longer field-lines and lower field strength [*Mozer*, 1970, 1973; *Kelley*, 2009]. The propagation time of an Alfvén wave between the ionosphere and the magnetic equatorial plane in the inner magnetosphere is typically on the order of tens of seconds [e.g., *Baumjohann and Treumann*, 1997].

[4] The Earth's plasmasphere has been observed to rotate at rates other than perfect corotation [*Sandel et al.*, 2003; *Gallagher et al.*, 2005; *Galvan et al.*, 2008]. At $L \sim 2$–3, plasmaspheric notches, azimuthally defined regions of low plasmaspheric density as observed in EUV images, have been previously observed to rotate at rates as low as 44% of corotation, though typical rates tend to be between 85% and 100% [*Sandel et al.*, 2003; *Gallagher et al.*, 2005]. These typical rotation rates are much slower than can be explained by outward transport of plasma as discussed by *Hill* [1979], which predicts that the effect of inertial lag would not become significant for the Earth inside of $L \sim 64$. Since the magnetospheric convection electric field dominates the Earth's corotation electric field at $L \sim 2$–7 (depending on geomagnetic activity levels), inertial lag is thought to be insignificant at the Earth.

[5] *Burch et al.* [2004] suggested that westward ionospheric drift causes plasmaspheric subcorotation, and hypothesized that the ionospheric drift is due to the ionospheric disturbance dynamo, though they were unable to fully test this hypothesis. In short, the disturbance dynamo, as described by *Blanc and Richmond* [1980], begins with the input of energy into the auroral zone by particle precipitation. The subsequent Joule heating leads to equatorward winds that move thermospheric gas to lower latitudes, where the velocity of the rotating Earth is higher due to greater distance from the spin axis. As the neutral gas moves equatorward out of the auroral zone, it conserves angular momentum by turning westward, thereby reducing angular velocity and lagging behind the rotation of the Earth. The westward wind produces a corresponding westward drift in the ionized plasma, so that the plasma also subcorotates. *Burch et al.* [2004] showed that this lag indeed occurs in ionospheric plasma equatorward of the auroral zone using DMSP ion drift meter (IDM) measurements, and that plasmaspheric subcorotation, obtained by tracking a plasmaspheric notch in EUV images, approximates ionospheric subcorotation in one example. *Gallagher et al.* [2005] examined 12 more cases, comparing EUV-determined plasmaspheric notch drift rates to DMSP IDM measurements and found that most showed the same correlation, though two of them notably did not. *Gallagher et al.* [2005] suggested that the dawn-dusk asymmetry in convection electric potential must be invoked to explain those cases where plasmaspheric subcorotation is not correlated with ionospheric westward drift. Although these previous studies have shown that plasmaspheric subcorotation is often correlated with westward ionospheric drift, the hypothesis that energy input into the auroral zone is the root cause of subcorotation has not yet been empirically tested. If true, one would expect to see a correlation between the rotation rate of the plasmasphere and the energy input into the auroral ionosphere.

[6] We present a statistical correlation analysis using up to 128 measurements of plasmaspheric rotation rate, extracted from IMAGE EUV data using two independent techniques, and a variety of geomagnetic and auroral indices, including *Dst*, *Kp*, *AE*, midnight boundary index (MBI), and Joule heating estimates from the assimilative mapping of ionospheric electrodynamics (AMIE) algorithm. We find a weak correlation between each of these indices and plasmaspheric rotation rate, but only for a subset of rotation rate measurements for which our two measurement techniques agree within 5%. In addition, the rotation rates derived from plasmaspheric features near dusk are generally slower than those from features near dawn, suggesting that both the dawn-dusk asymmetry in convection potential and the ionospheric disturbance dynamo contribute to the variability in plasmaspheric rotation rate, even deep within the inner magnetosphere ($L = 2.5$). Our analysis quantifies the variability of plasmaspheric rotation and includes the first known observation of plasmaspheric superrotation. Although *Rishbeth et al.* [1972] discussed superrotation of the Earth's upper atmosphere, the phenomenon has never been clearly observed in the plasmasphere.

2. Methodology

[7] The extreme ultraviolet (EUV) instrument on board the IMAGE spacecraft provided images of 30.4 nm sunlight resonantly scattered by He^+ in the Earth's plasmasphere between 2000 and 2005 [*Sandel et al.*, 2000]. We surveyed IMAGE EUV data from 2001, when the IMAGE spacecraft was at apogee over the Earth's north pole, a favorable geometry for viewing equatorial projections of the plasmasphere, and hence for tracking plasmaspheric features to determine rotation rate. We searched for intervals that had long duration continuous EUV observations, which allow for more reliable tracking of plasmaspheric features. The longest-duration high latitude IMAGE passes were centered about June 2001. We selected 128 IMAGE passes with a minimum duration of 6 h of clear EUV data, and an azimuthal plasmaspheric feature that could be tracked. The maximum duration of useful data in a single orbital pass was 10 h. Rotation rates were estimated for each 6–10 h IMAGE pass. The data selection was described in more detail by *Galvan et al.* [2008], as that study required the development of the same database to study the diurnal variation of plasmaspheric He^+ via flux tube tracking.

[8] Two methods were used to extract plasmaspheric rotation rates from EUV images: one automated and one manual. Both techniques first involve collecting EUV images of the plasmasphere from a selected IMAGE pass (an "event") and subtracting scattered sunlight and other noise effects. This background subtraction is carried out by first selecting a region of the EUV image that is outside the plasmapause, across all vertical pixel columns of the image. In each column, the pixels that are outside the plasmapause are averaged to produce a background radiance value, which is then subtracted from all pixels in that column. This technique helps to make the azimuthal features of the plasmasphere clearer so they can be more easily tracked in both the manual and automated techniques.

[9] Both methods also involve mapping the background-subtracted EUV images to the geomagnetic equatorial plane, then taking an azimuthal profile of radiance in a given range of L values. The process of mapping the image to the equatorial plane was first described by *Roelof and Skinner* [2000] and first applied to IMAGE EUV images by *Sandel et al.* [2003]. It uses dipole magnetic field geometry to re-position the radiance value of each pixel in the EUV image. The mapping process relies on the assumption that the plasmaspheric density drops off rapidly with increasing L, and that therefore the majority of the contribution to the observed radiance in a given EUV pixel is due to He^+ ions at the lowest L values along the line of sight. This assumption could be violated in the case of plasmaspheric plumes, which can result in increasing density with L in certain regions of L and local time [e.g., *Spasojević et al.*, 2003; *Goldstein et al.*, 2004; *Gallagher et al.*, 2005]. Also, the real geomagnetic field geometry can differ significantly from a dipole, especially at higher L and in periods of intense geomagnetic activity [e.g., *Berube et al.*, 2006]. Since both violations would result in reduced accuracy of the equatorially mapped EUV images, primarily in the radial position of the mapped radiance values, we concentrate on relatively low L values for this study (L of 2.5 and 3.5), where any inaccuracies inherent to the mapping process should be minimal, and where geomagnetic activity is less likely to strongly influence the field geometry. Also, our procedure for tracking the rotation rate of the plasmasphere relies on observing features with azimuthal (not radial) brightness variation, and so should be largely unaffected by uncertainties in the equatorial mapping routine.

[10] For this study, we focused on L shell ranges of 2.25–2.75 (centered at L = 2.5) and 3.25–3.75 (centered at L = 3.5). We overlaid a circular annulus surrounding the Earth on the equatorially mapped EUV image, indicating which pixels fall within those L shell ranges (one annulus centered at L = 2.5, and one at L = 3.5). We then extracted the average radiance as a function of magnetic local time (MLT) from the EUV pixels within those annuli. For all 128 of our EUV events, the azimuthal annulus ranging from L = 2.25 to 2.75 was well within the overall plasmapause, excepting those trackable azimuthal features, such as "notches," which bring the gradient between high and low density to lower L shells within a localized region of MLT. Such trackable features could be argued to represent the plasmapause itself in a particular MLT region, but we consider them as separate features from the general plasmapause observed at other local times. For 91 of those 128 events, the annulus ranging from L = 3.25 to 3.75 was within the overall plasmapause as well. There are more events that have the L = 2.5 annulus fully contained within the plasmasphere than at L = 3.5, as the location of the plasmapause varies with geomagnetic activity, and more frequently moves within L = 3.5 than L = 2.5. By keeping the annuli within the overall plasmapause, we reduce the likelihood that a general inward motion of the plasmaspause, due to increasing geomagnetic activity, would contaminate the profile with brightness variations that are not due to azimuthal features rotating with the plasmasphere. Thus, for all events used in this study, the only large gradients in EUV radiance are due to the azimuthal features we are tracking to monitor the rotation rate, as we have verified our radiance profiles are not contaminated with other plasmapause crossings.

[11] In the automated technique, the azimuthal radiance profile of one image is cross-correlated with the profile from an image taken at a later time. If the azimuthal feature being tracked is prominent enough, the maximum correlation coefficient between the two profiles will occur at a lag value that corresponds to the local time traversed by the feature. This change in local time can then be compared with the change in universal time between the two images. Dividing the change in local time by the change in universal time yields a corotation factor, which will be 1 for a perfectly corotating plasmasphere. Values below 1 correspond to subcorotation, and values greater than 1 correspond to superrotation.

[12] During an IMAGE pass that lasts 9 h, for instance, we would take 10 images, one every hour. For each pair of images, the cross correlation may yield a slightly different corotation factor. In addition, our precision is limited by the azimuthal resolution of the EUV images. The annulus used in obtaining radiance profiles is broken into 128 azimuthal bins, each 11.25 min of local time in width. Higher resolutions could lead to bin width approaching EUV pixel size, and so are not used. Corotation factors obtained in this way have a precision uncertainty of 11.25 min (local time) divided by the difference in universal time between the two images. Hence, our precision uncertainty is lower for a larger time difference between the images. In order to obtain an average corotation factor that can be assigned to the entire event, we compute a corotation factor from each pair of images separated by more than a minimum duration of universal time, and take the weighted mean. That minimum duration is determined by the minimum desired precision uncertainty; in this case, we require that our corotation factors be precise within ±5% of corotation. Thus, our minimum allowable duration between images is 11.25 min/0.05 = 3.75 h. Any pair of images in our event separated by more than 3.75 h produces a corotation factor that will be included in the weighted mean. This method of determining the corotation factor is discussed in more detail by *Galvan et al.* [2008].

[13] The manual technique of measuring plasmaspheric rotation rates involves visually surveying the azimuthal radiance profiles extracted from the EUV images and recording the location of a plasmaspheric feature such as a "notch," "crenulation," "finger," or "shoulder." These terms reference specific plasmaspheric features observed and discussed by *Sandel et al.* [2003] and summarized by *Darrouzet et*

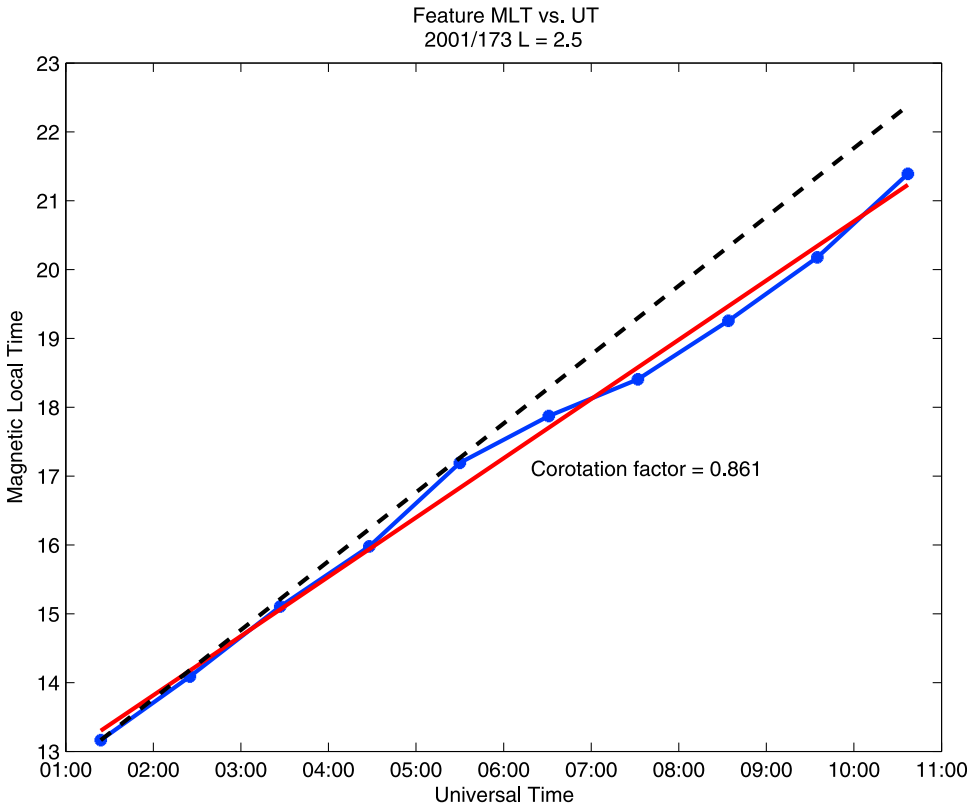

Figure 1. An example of corotation factor determination using the technique of visually tracking a rotating plasmaspheric feature. Each dot is the position in LT and UT of a plasmaspheric feature being visually tracked in brightness profiles extracted from EUV images. The dashed line represents perfect corotation (slope = 1). The solid straight line represents a least squares fit to the positions over the entire event, the slope of which is taken to be the corotation factor for that event.

al. [2008], which may be tracked to infer the rotational motion of the plasmasphere. Since a plasmaspheric feature may potentially have a varying rotation rate depending on *L*-value, we used the radiance profiles extracted from each background-subtracted EUV image to track the features, as these profiles are *L* shell specific and will result in corotation factors that are more directly comparable to those generated in the automated technique. The marked position of a plasmaspheric feature in local time and universal time is recorded from each hourly image profile in an event, and the differences in those positions between images represent corotation factors. Figure 1 shows an example of recorded LT and UT positions for a feature tracked in the event day 173, UT 01:24–10:37. Although the individual corotation factors between images, represented by the slope of the line segments between each point, may differ significantly over an event, we obtain an average corotation factor over that IMAGE pass by taking a least squares fit to the feature positions, and using the slope of the fit line as the corotation factor. Again, because we are visually tracking features in the same radiance profiles that were used in the automated technique, our precision uncertainty for each individual corotation factor is the 11.25 min bin width of the azimuthal annulus divided by the difference between EUV images in universal time.

[14] The uncertainty for the least squares fit value is the uncertainty of the weighted mean, equal to $\sqrt{1/\sum \sigma_i}$, where σ_i is the individual uncertainty (11.25 min/60 min/hr)/ Δ UT. Since each of the individual corotation factors from this technique comes from visually tracking a feature between two images spaced 1 h apart in UT, the individual precision uncertainties are (11.25 min/60 min =) ± 0.19. These individual precision uncertainties contribute to the error of the weighted means, which are used as the error bars for our plots of the corotation factors (Figures 4 and 5, discussed in section 3.1). The manual corotation factors generally have larger error bars than the automated corotation factors, because the Δ UT between images compared in the manual technique are typically 1 h, whereas the automated technique limits the individual corotation factors used to those where the UT difference is generally above 3.75 h, as discussed earlier in this section.

[15] Note that our choice to use the error of the mean as a representation of the uncertainty in our corotation factor measurements is based on the idea that the mean corotation factor for a given event (or the least squares fit, in the case of the manual technique) is more representative of the true plasmaspheric rotation rate than any of the individual corotation factors determined between a given pair of images. As such, the error of the mean speaks to the stability of the value

of the mean, which we take as the corotation factor for a given event. An alternative would be to use the standard deviation of the individual corotation factors about the mean as a representation of uncertainty. This would speak to the variability of the individual corotation factors in each event, and was typically ~±0.20 for most events, but in a few extreme cases was as high as ±0.48. Although the standard deviation gives useful information about the variability of the measured individual corotation factors for a given event, those apparent variations in rotation rate during a single 6–10 h time period are unlikely to represent real geophysical changes, and are more likely due to measurement uncertainty. Because we take the mean or least squares fit of those individual corotation factors to be a more physically reliable estimate of the plasmasphere's rotation for that event, we choose the uncertainty in the value of the mean as an appropriate indication of the expected error in the final corotation factors.

[16] Once corotation factors were collected using both techniques, we compared the measurements taken with the two techniques for the same events. The two measurements taken for each event may differ from each other because of a variety of reasons, including local time variation of rotation rate, different features in the same radiance profiles moving at slightly different rates, the changing morphology of plasmaspheric features over time, and the limited precision and accuracy in each of the techniques. We surmise that those events for which both techniques yield essentially the same corotation factor to within the precision of 5% of corotation provide the most reliable estimates of the rotation rate of the plasmasphere, and hence these particular events are compared with the geomagnetic and auroral indices as a separate data set.

[17] The *AE* index is a measure of global auroral electrojet activity, as originally introduced by *Davis and Sugiura* [1966]. The MBI is a measure of the equatorward boundary of precipitating auroral electrons at midnight local time as measured by particle detectors on board the DMSP spacecraft [*Gussenhoven et al.*, 1981]. We chose the *AE* and MBI indices to compare with our corotation factors because these indices should give some measure of the energy input to the auroral zone. If the suggested model of *Burch et al.* [2004] is correct, and subcorotation is a result of particle precipitation and Joule heating in the auroral zone, then our corotation factors should show some correlation with auroral activity. We also compared with measures of geomagnetic activity. The *Kp* and *Dst* indices measure variations in ground-based magnetic observatories due to geomagnetic disturbances and the intensity of the ring current, respectively, and are used in this study as an indication of overall geomagnetic activity. We also compare our measured rotation rates with estimates of Joule heating for the northern hemisphere produced by the AMIE algorithm, which assimilates data from superDARN radar, ground-based magnetometers, and electric field measurements from the DMSP satellites [e.g., *Lu et al.*, 2001]. We also make a visual survey of images of the proton aurora from the IMAGE FUV instrument to observe auroral activity in the 24 h preceding a subset of our corotation measurements. Global images of auroral activity can give an indication of the intensity of particle precipitation and, presumably, subsequent Joule heating. Finally, among our measurements of the plasmasphere's rotation rate, we observe at least two cases of superrotation in the plasmasphere based on EUV images, and corroborate these observations by checking DMSP IDM measurements of eastward ionospheric drifts.

3. Results

3.1. Statistics of Observed Rotation Rate

[18] Figure 2 shows the distributions of corotation factors obtained with both the automated and manual techniques, at $L = 2.5$ and $L = 3.5$. Corotation factors were extracted from 128 events with the automated technique and 119 events with the manual technique at $L = 2.5$. At $L = 3.5$, corotation factors were extracted from 91 events with the automated technique and 90 events with the manual technique. The manual technique produced fewer corotation factors than the automated technique because certain plasmaspheric features were too difficult to distinguish visually. Figure 3 shows the same distributions, but filtered to include only those events for which the corotation factors determined from the two methods were within 0.05 of one another. Thirty-one events met this condition at $L = 2.5$, and 25 met it at $L = 3.5$. Table 1 shows the statistical data for all eight histograms presented.

[19] Although the rotation rates are more accurately known for those events in which both techniques result in roughly the same corotation factor than for those events in which the two techniques produce significantly different corotation factors, it is worth noting that the mean and median corotation factor values of the filtered distribution and the non-filtered distribution are within 0.03 of each other. Thus, statistical data from the full data set and the filtered subset tell the same story: the average state of the plasmasphere is slight subcorotation with inferred mean corotation factors ranging from 0.88 to 0.95, depending on measurement technique and L shell. The plasmaspheric rotation rate is generally lower at higher L shells.

[20] Figures 4 and 5 show the corotation factors obtained at $L = 2.5$ from the manual and automated techniques, respectively, as a function of universal time (the middle time for each event is used), each with error bars representing the uncertainty discussed in the methodology section. There does not appear to be a significant trend in rotation rates over the period of observation. Figure 6 shows the differences between corotation factors obtained with the two different techniques at $L = 2.5$, with error bars representing their added uncertainties. The center horizontal line represents a difference of zero, where the two techniques produce exactly the same corotation factor. The upper and lower horizontal lines represent a difference of ±0.05, such that all points between those lines represent the events making up the "filtered" distribution of rotation rate measurements. A similar analysis of corotation factors at $L = 3.5$ did not reveal any trends over the period of observation.

3.2. Comparisons With Indices

[21] These corotation factors were compared with *Dst*, *Kp*, *AE*, and MBI indices, estimates of hemispheric Joule heating from the AMIE model, as well as a visual survey of the proton aurora activity level as observed in IMAGE FUV images. In general, we found a weak correlation between higher levels of geomagnetic activity and lower corotation factors, but only when analyzing the filtered subset of events for which the two techniques produced corota-

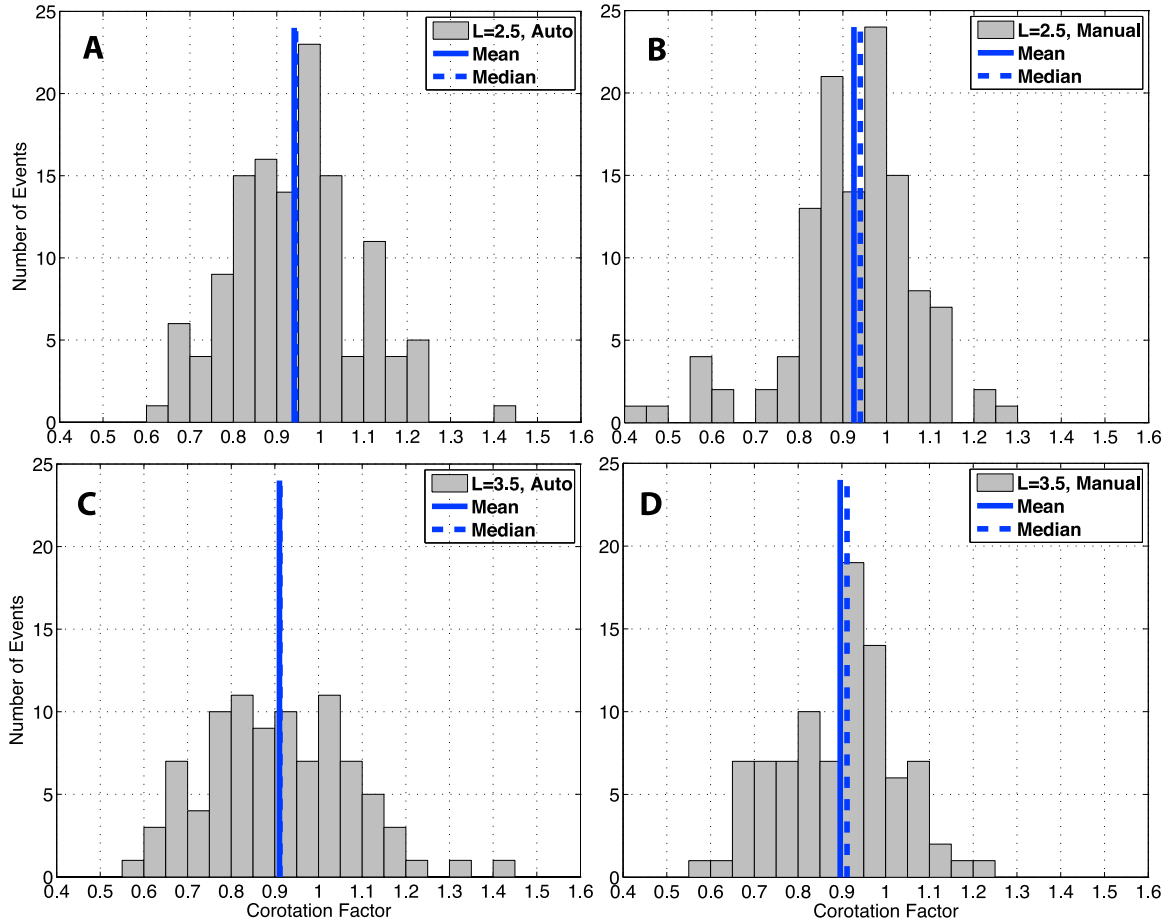

Figure 2. Distributions of corotation factors from the (a and c) automated and (b and d) manual techniques at L = 2.5 and L = 3.5. Figures 2a and 2c show the automated technique at L = 2.5 and L = 3.5, respectively. Figures 2b and 2d show the manual technique at L = 2.5 and L = 3.5, respectively.

tion factors within 0.05 of one another. As such, we focus our discussions on comparisons for the filtered subset of events in this paper, as comparisons with the full data set of corotation factors yielded no significant correlations. We operate under the assumption that this filtered subset of events represents rotation rate measurements that are more accurate than those of the unfiltered data set, which includes many events where the two measurement techniques, automated and manual, produced rotation rates that are significantly different from one another, as seen in Figure 6.

[22] Figure 7 shows five scatterplots of corotation factor plotted against a particular index of geomagnetic or auroral activity, or the estimates of Joule heating. These plots show correlation tests for the full data set of 128 events used in the automated technique at L = 2.5. A least squares linear fit is applied in each of the plots, to illustrate the direction of a crude linear relationship, if one exists. The legends in Figure 7 show R, the linear correlation coefficient for that comparison, and the P value, which indicates the probability of obtaining that correlation coefficient from points selected from a random parent distribution. A typical rule of thumb is to consider a correlation coefficient significant if the associated P value is smaller that 5%, or 0.05 [e.g., *Bevington and Robinson*, 2003]. The smallest P value displayed in Figure 7 is 0.131, and its associated R value is a very low −0.134, in the comparison with Joule heating estimates. This indicates that none of the shown comparisons yield any significant correlations between plasmaspheric rotation rate and the indices of geomagnetic activity or Joule heating. These plots are typical of most of the comparisons performed in this study, showing no significant correlation.

[23] Table 2 shows R and P values for all comparisons performed in this study. Note that the only correlation tests with P values below 0.05, highlighted in bold, are those for the filtered subset of events for which the two measurement techniques yielded corotation factors within 0.05 of one another, and only for L = 2.5. We find no significant correlation between corotation factor and any of the indices or estimates of Joule heating at L = 2.5 or L = 3.5 when using the full data set of corotation factors determined using either technique.

[24] We now focus on those comparisons that did yield weak correlations between activity levels and corotation factor. Figure 8 shows four scatterplots, each comparing the filtered subset of corotation factors with the summed *Kp* (Figures 8a and 8c) or summed *Dst* (Figures 8b and 8d) over the 24 h preceding the events, at both L-shells. All corotation factors shown were generated using the manual technique, but recall that these are events for which both

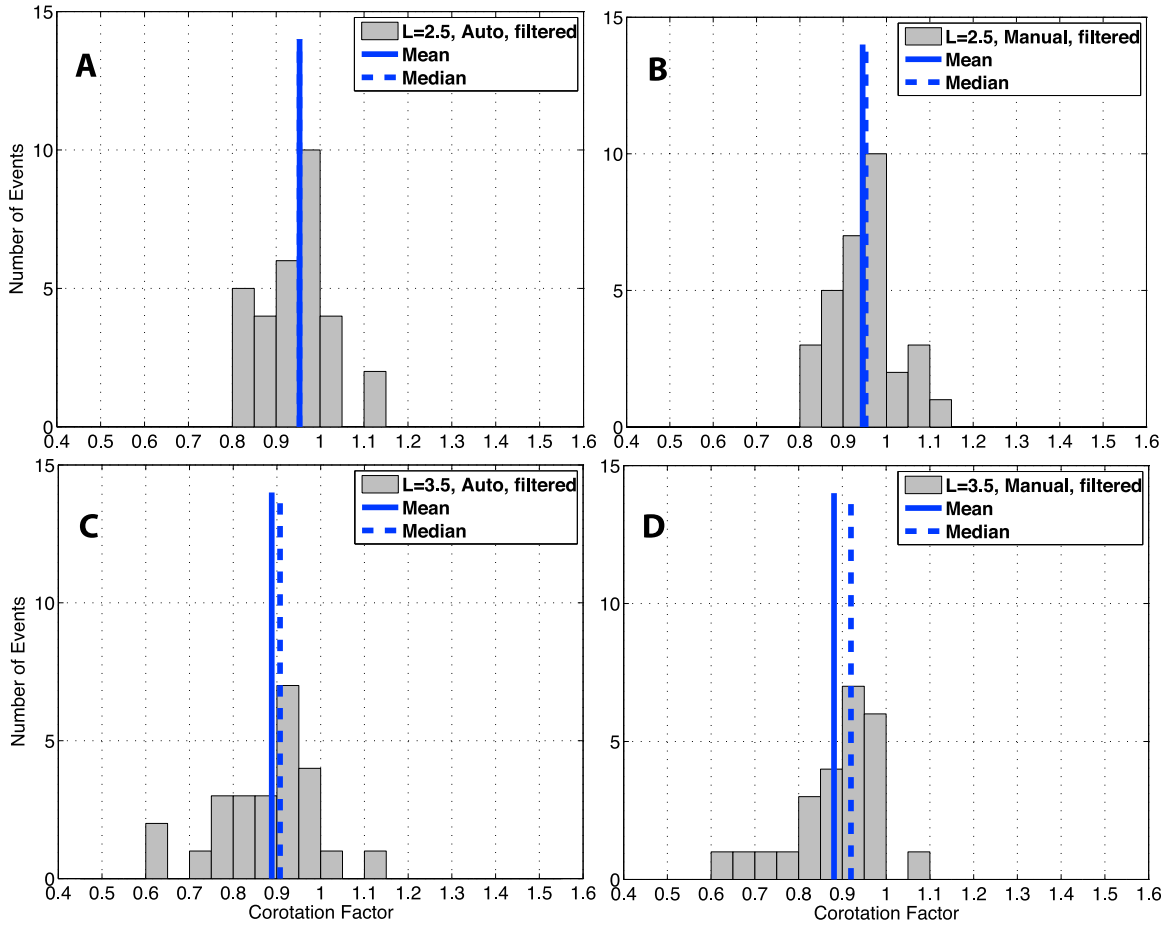

Figure 3. Same as Figure 2, but for only those events in which the corotation factors determined by the two methods were within 0.05 of one another. (a) The automated technique at L = 2.5. (b) The manual technique at L = 3.5. (c) The automated technique at L = 3.5. (d) The manual technique at L = 3.5.

techniques yielded corotation factors within 0.05 of one another, so plots showing the corotation factors generated using the automated technique would look very similar. The correlation coefficient is 0.441 for the *Kp* comparison and 0.462 for the *Dst* comparison at L = 2.5; but notice that the P values put the probability that these correlations coefficients were obtained by random chance at near 1%. Hence, we would describe the correlation between the rotation rate of the plasmasphere and the geomagnetic indices (*Kp* and *Dst*) summed over the 24 h preceding the event as weak (due to the fairly low correlation coefficients), but significant (due to the low P value). Low summed *Dst* values weakly correlate with low corotation factors, implying that high ring current intensity correlates with subcorotation at L = 2.5. In turn, high *Kp* values weakly correlate with low corotation factors, implying that high geomagnetic activity correlates with subcorotation. At L = 3.5, the correlation coefficients are much lower and the P values high enough to imply that there are no significant correlations at this L-shell.

[25] Figure 9 shows similar plots comparing the corotation factors with average MBI (Figures 9a and 9c) and summed *AE* (Figures 9b and 9d) values from the 24 h preceding the events. Although Figure 8 shows the correlation between plasmaspheric rotation rate and geomagnetic activity, the comparisons of Figure 9 address the correlation between rotation rate and auroral energy input. As with *Dst* and *Kp*, at L = 2.5 there appears to be a weak but significant correlation between rotation rate and average MBI, as well as summed *AE*, in the 24 h preceding the event. Typically, high summed *AE* values correspond to subcorotation, as do low values of average MBI. This correlation, though weak, is consistent with the hypothesis of *Burch et al.* [2004], because high *AE* and low MBI would

Table 1. Statistical Data for Measurements of Plasmaspheric Rotation Rate

Technique	L	N	Mean Corotation Factor	Standard Deviation	Median
Automated	2.5	128	0.94	0.15	0.94
Manual	2.5	119	0.93	0.15	0.94
Automated	3.5	91	0.91	0.16	0.91
Manual	3.5	90	0.90	0.13	0.91
Automated (filtered 0.05)	2.5	31	0.94	0.08	0.95
Manual (filtered 0.05)	2.5	31	0.95	0.07	0.95
Automated (filtered 0.05)	3.5	25	0.88	0.11	0.92
Manual (filtered 0.05)	3.5	25	0.89	0.10	0.91

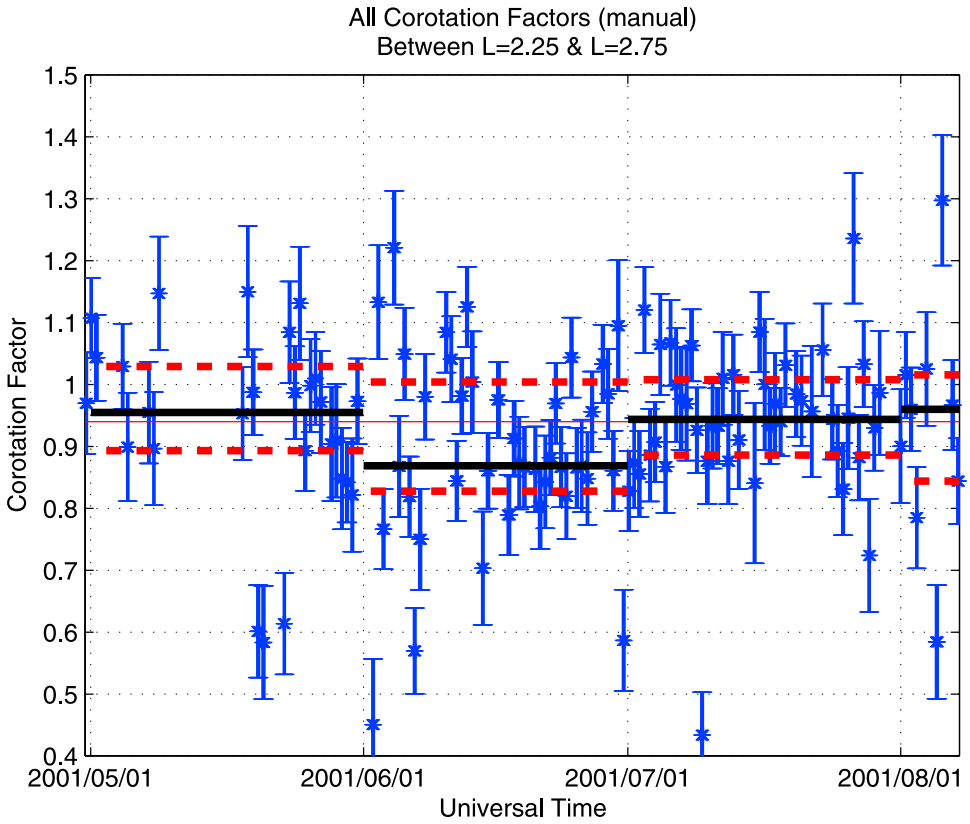

Figure 4. Manual corotation factors for $L = 2.5$. The long horizontal line is the median corotation rate across the entire observation period. The shorter lines are the monthly binned medians, with dashed lines showing upper and lower quartiles.

be associated with greater auroral activity and Joule heating of the ionosphere, and hence equatorward winds and subcorotation. Again, the correlations are only significant at $L = 2.5$, and the comparisons for rotation rate measurements taken at $L = 3.5$ show no significant relationship between the auroral indices and corotation factors. Figure 10 shows similar scatterplot comparisons between corotation factor and summed estimates of Joule heating from the AMIE model in the 24 h preceding the event, in units of gigawatts. Again, we see a weak but significant correlation at $L = 2.5$, but none at $L = 3.5$. This observed correlation is also supportive of the hypothesis that the ionospheric disturbance dynamo is a cause of subcorotation, as higher hemispheric Joule heating estimates are correlated with lower corotation factors.

[26] Our filtered event corotation factors still have significant variability, as can be seen in Figures 8–10, and we are interested in the precision of our R values for those comparisons that show a weak correlation. We perform a "bootstrapping" analysis to further investigate the degree to which outliers influence the calculated correlation coefficients. Figure 11 shows bootstrap histograms for each of the correlation tests at $L = 2.5$ for the filtered subset of data. The bootstrapping technique works by randomly resampling out of our data set, with replacement, and generating a correlation coefficient for the resampled data [e.g., *Reiff*, 1990]. This process is repeated one thousand times for a given comparison between corotation factor and one of the indicators of geomagnetic or auroral activity. The histograms show the distribution of R values obtained from this process. A broad distribution indicates that the correlation coefficient is highly influenced by outlying data points, whereas a narrow distribution indicates that outliers have a negligible effect. All of the histograms in Figure 11 show a fairly broad distribution, owing to the fact that there is considerable scatter in the data shown in Figures 8–10. Thus, omitting any one of the many outliers in the small subset of data (31 events) can significantly affect the calculated correlation coefficient. However, we note that the 95% confidence intervals are either completely positive or completely negative for each histogram. If there truly were no significant correlation, the distribution of R values generated by the bootstrapping test would likely have a significant number of both positive and negative possible correlation coefficients. Instead, the vast majority of each distribution is either positive or negative. For instance, the distribution for the comparison with Joule heating shows a 95% confidence interval of between −0.68 and −0.24, meaning that the true value of the correlation coefficient between corotation factors and Joule heating is likely to be within that range. A negative correlation in that range would mean that increased Joule heating was (weakly) correlated with subcorotation, as suggested by *Burch et al.* [2004]. It is highly unlikely that the significant correlation coefficients for these comparisons, listed in Table 2, came about by accident, especially because the multiple comparisons tend to confirm one other. Hence, although the observed correla-

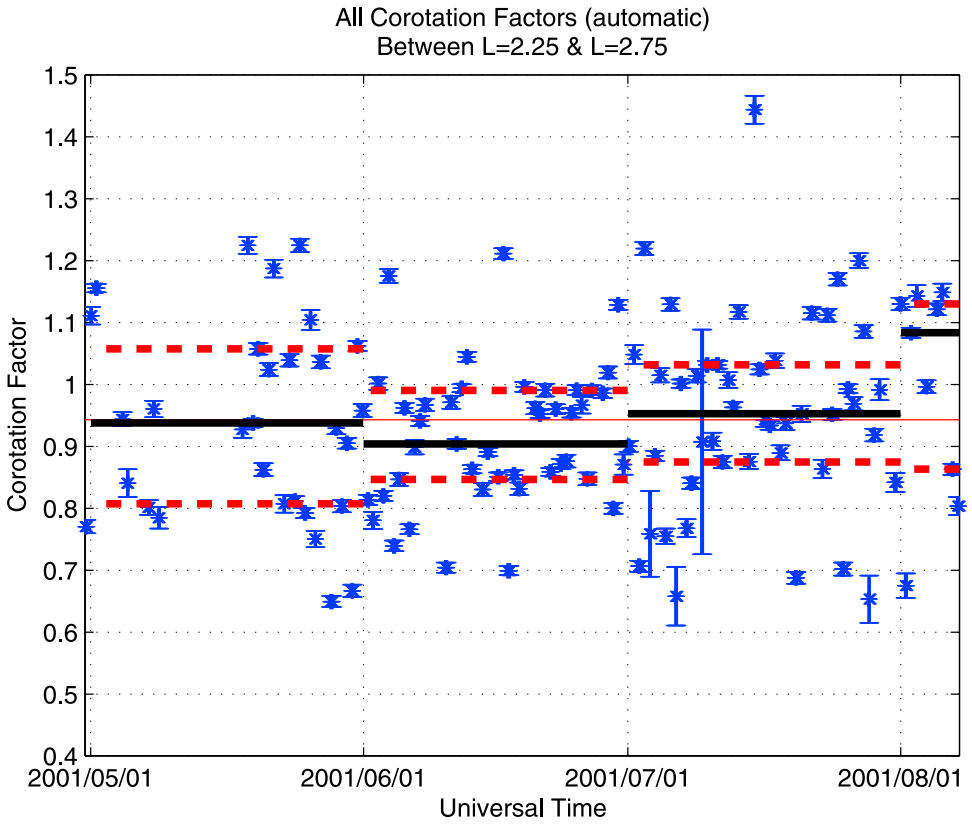

Figure 5. Automated corotation factors for $L = 2.5$. The long horizontal line is the median corotation rate across the entire observation period. The shorter lines are the monthly binned medians, with dashed lines showing upper and lower quartiles.

tions are certainly weak, there is a significant relationship between corotation factor and our indices of activity and Joule heating at $L = 2.5$.

3.3. FUV Images

[27] We made a visual survey of IMAGE FUV images of the proton aurora in the 24 h preceding each of the events in the filtered data set for $L = 2.5$. The radiance in an FUV image depends not only on auroral precipitation but also on airglow and viewing geometry, resulting in a large potential error source that is difficult to remove. As such, no standardized index has been developed to estimate Joule heating based on FUV auroral observations (Harald Frey, personal communication, 2008). Without a standardized index, we looked for periods of intense sustained aurora in the 24 h preceding a given corotation factor event, and grouped our observations into categories of "no activity," "mild activity," "moderate activity," and "intense activity" in the 24 h preceding each event. After comparing these observations with our corotation factors, we observed no correlation with plasmaspheric rotation rate. Given the subjectivity inherent in classifying the FUV auroral observations in this way, we abstain from drawing conclusions from our FUV image survey and suggest that the MBI provides a more consistent and appropriate index of auroral activity for this study, as a low average MBI indicates an expanded auroral oval. In addition, the hemispheric results from AMIE provide robust estimates of Joule heating, reducing the need to use FUV data as a Joule heating proxy.

3.4. Local Time Dependence

[28] Finally, we examine the magnetic local time (MLT) distribution of the features tracked in the manual technique for measuring plasmaspheric rotation rate. Figures 12 and 13 show the corotation factors versus magnetic local time of the feature being tracked for $L = 2.5$ and $L = 3.5$, respectively. These comparisons are only available for the manual technique because this technique tracks a specific feature in the plasmasphere, whereas the automated routine cross-correlates the entire EUV brightness profile across all MLTs. The individual points in Figures 12 and 13 represent the individual corotation factors between each position in UT and MLT of a feature being tracked visually in the EUV radiance profiles, corresponding to the slopes of the short line segments between data points in Figure 1. Using an average corotation factor over a 6–10 h event would result in an ambiguous local time association, or at best a range of local times; hence, we chose to use the individual 1 h resolution corotation factors to monitor MLT dependence, plotting the factors at the average MLT between the observed feature position in the EUV radiance profile. The short horizontal solid lines show the mean corotation factor value in 3 h bins of MLT. At both L shells, the mean corotation factor drops significantly near dusk as compared with the means from

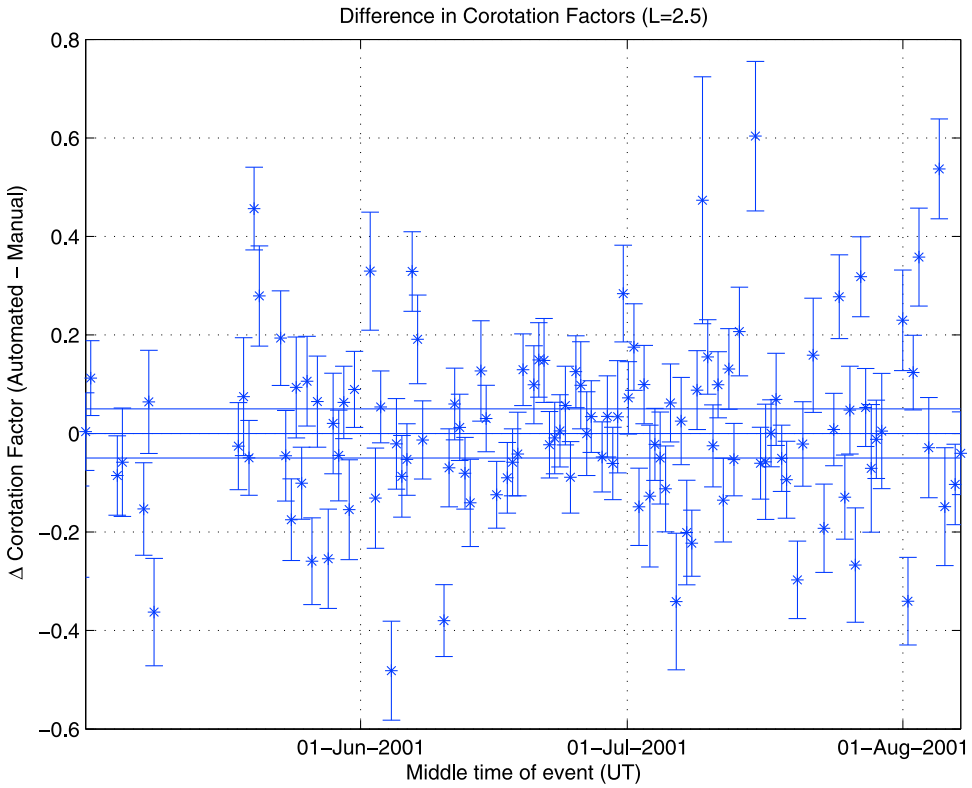

Figure 6. Difference between corotation factors produced by two different techniques at $L = 2.5$. The upper and lower horizontal lines mark ±0.05. Events for which the difference is within these boundaries are considered as a separate subset of data.

dawn through the afternoon. The effect is more prominent at $L = 3.5$. Also, there appears to be a minimum in rotation rate on the nightside in the $L = 2.5$ data, and at $L = 3.5$ the minimum is closer to dusk.

4. Discussion

[29] For those events in which the two different measurement techniques yielded corotation factors within 0.05 of one another, there is a weak but significant correlation with auroral and geomagnetic activity. Lower corotation factors are generally associated with higher auroral and geomagnetic activity, manifested in higher summed Joule heating estimates from AMIE, higher summed *Kp* and *AE* indices and lower average MBI and summed *Dst* indices in the 24 h preceding each event. This correlation is consistent with the hypothesis of *Burch et al.* [2004] that auroral heating during periods of high geomagnetic activity can lead to equatorward thermospheric winds that cause subcorotation of ionospheric plasma at midlatitudes. Interestingly, this correlation is only apparent at $L = 2.5$ and does not appear at $L = 3.5$. In addition, when we examine the entire, unfiltered data set of corotation factors, no geomagnetic dependence is apparent. This suggests several possible conclusions. It may be that we are unable to determine the plasmaspheric rotation rate to the necessary accuracy in many cases; a possibility supported by the fact that the expected trend only becomes visible when we regard the subset of events for which both measurement techniques gave consistent values.

[30] Another possibility is that the effect described by *Burch et al.* [2004] is not the only important phenomenon leading to variable rotation rate. As we see in Figures 12 and 13, magnetic local time plays a role in plasmaspheric rotation rate as well. Because the superposition of corotation and convection electric fields leads to E × B drift directions that are the same on the dawnside and opposite on the duskside, one would expect the plasmasphere to rotate faster on the dawnside and slower on the duskside. Although this effect would lead to different measured corotation factors at dawn versus dusk, as we observed in this study, the net rotation rate of the plasmasphere over a full rotation should average out to corotation if the convection electric field is roughly the same strength at both dawn and dusk meridians. However, *Gallagher et al.* [2005] discussed a dawn-dusk asymmetry in the magnetospheric electric potential pattern as another possible cause of subcorotation. They note that *Lu et al.* [1989] found the potential difference between the magnetic pole and the equator along the dusk meridian is typically 1.5 times larger than the potential difference along the dawn meridian, a phenomenon likely caused by the Hall conductance gradient at the terminators, which reduces the magnitude of the dawnside potential peak and increases the size of the duskside potential well [*Ridley et al.*, 2004]. With such a potential asymmetry, there would be a stronger sunward convection on the duskside than on the dawnside, resulting in a net subcorotation over a given rotation. *Liemohn et al.* [2004] showed that this dawn-dusk asymmetry varies with storm phase, likely due to changes in field-aligned current and

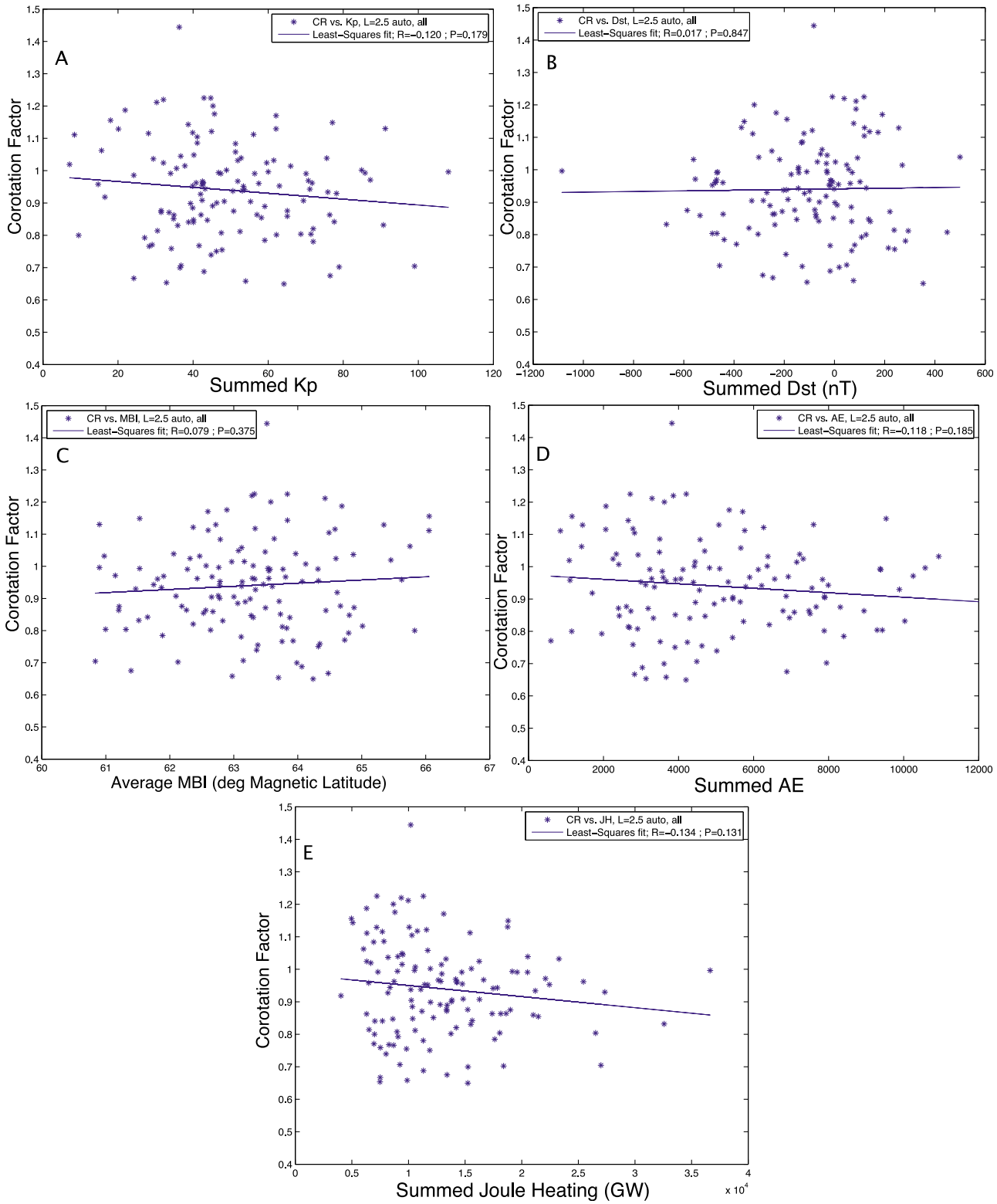

Figure 7. Corotation factor, for all events using the automated technique, plotted versus (a) summed *Kp*, (b) summed *Dst*, (c) average MBI, (d) summed *AE*, and (e) summed Joule heating from the AMIE model in the 24 h preceding the event. High *P* values (>0.05) show that no significant correlations are apparent.

ionospheric conductivity, such that the asymmetry would be stronger in the main phase of the storm, and weaker during the recovery phase. All of this implies that the rotation rate of the plasmasphere depends both on local time and magnetospheric storm phase, in addition to any influence by the ionospheric disturbance dynamo as suggested by *Burch et al.* [2004]. Both magnetospheric convection and ionospheric winds affect the dynamics of the plasmasphere.

Table 2. Correlation Coefficients *R* and *P* Values Between Rotation Factors and Various Indices[a]

Technique	*L*	*N*	*AE R* (*P*)	MBI *R* (*P*)	JH *R* (*P*)	*Kp R* (*P*)	*Dst R* (*P*)
Automated	2.5	128	−0.118 (0.185)	0.079 (0.375)	−0.134 (0.131)	−0.120 (0.179)	0.017 (0.847)
Manual	2.5	119	0.004 (0.962)	−0.009 (0.920)	−0.034 (0.711)	0.020 (0.827)	−0.080 (0.384)
Automated	3.5	91	0.031 (0.769)	0.016 (0.880)	−0.030 (0.779)	−0.119 (0.261)	−0.037 (0.726)
Manual	3.5	90	−0.038 (0.720)	0.090 (0.400)	−0.050 (0.638)	−0.109 (0.307)	0.019 (0.859)
Automated (Filtered 0.05)	2.5	31	**−0.502 (0.004)**	**0.514 (0.003)**	**−0.489 (0.005)**	**−0.441 (0.013)**	**0.477 (0.007)**
Manual (Filtered 0.05)	2.5	31	**−0.510 (0.003)**	**0.457 (0.010)**	**−0.493 (0.005)**	**−0.441 (0.013)**	**0.462 (0.009)**
Automated (Filtered 0.05)	3.5	25	−0.098 (0.641)	0.211 (0.312)	−0.012 (0.955)	−0.185 (0.376)	−0.033 (0.875)
Manual (Filtered 0.05)	3.5	25	−0.075 (0.722)	0.198 (0.344)	0.032 (0.879)	−0.166 (0.429)	−0.032 (0.880)

[a]*P* values are given in parentheses. Cases with *P* values less than 0.05 are in bold, indicating a significant correlation. JH is Joule heating estimates from AMIE.

[31] The relative contributions of these different processes to the variability of the plasmaspheric rotation rate are difficult to determine based on our current study. The dawn-dusk asymmetry effect should be storm phase dependent, which should lead to a correlation between our corotation factors and the *Dst* and *Kp* indices summed over the preceding 24 h. Higher magnitudes of summed *Kp* and *Dst* values would imply more frequent or powerful magnetospheric storm activity in that 24 h time period, and thus more time during which the dawn-dusk asymmetry could have contributed to subcorotation. We do observe such a correlation, as seen in Figure 8, but only for the filtered events, only at $L = 2.5$, and the correlation itself is not very strong. A significant number of measurement events have low corotation

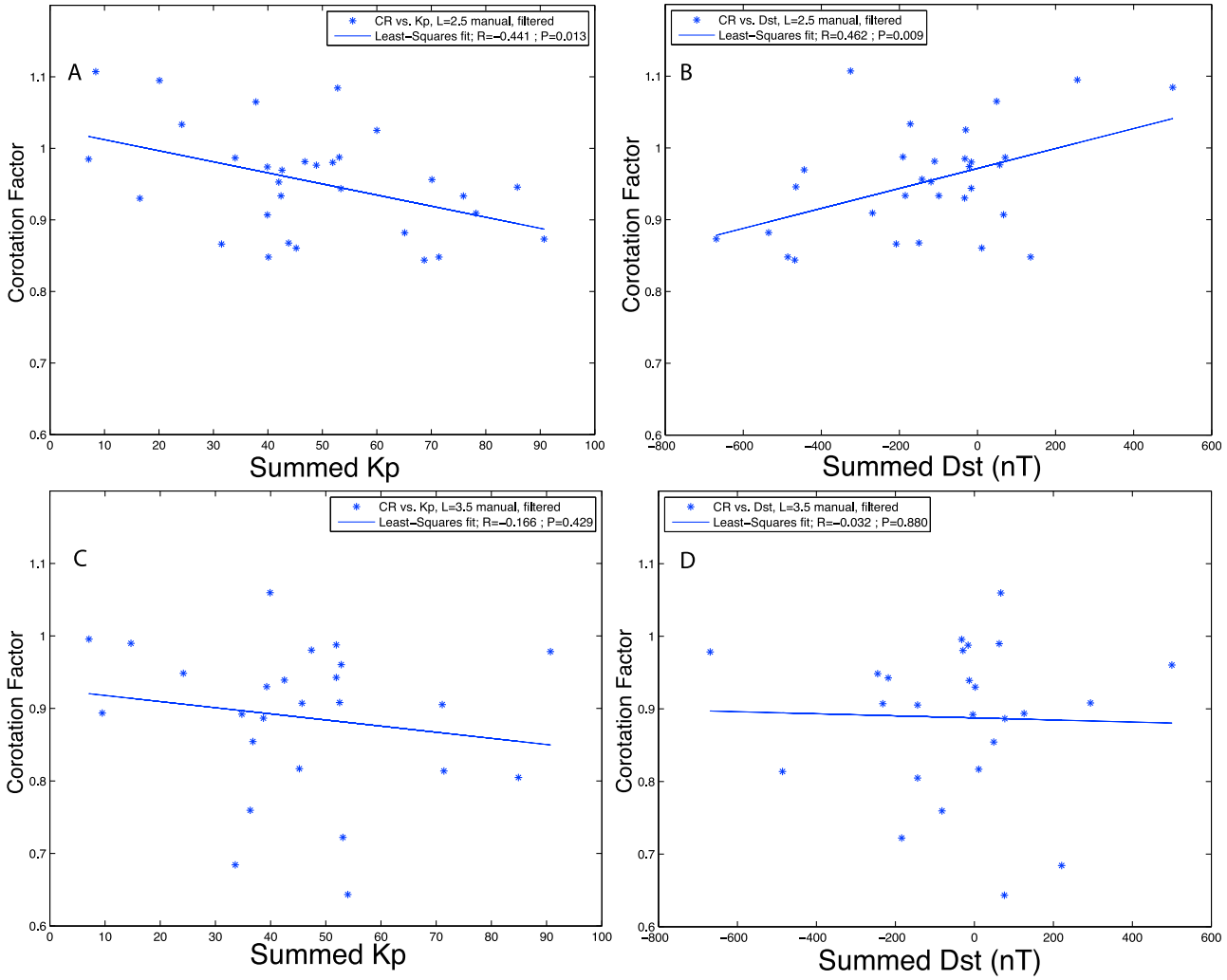

Figure 8. Corotation factor, for filtered events only, (a and c) plotted versus summed *Kp* and (b and d) summed *Dst* in the 24 h preceding the event. Shown for $L = 2.5$ in Figures 8a and 8b and $L = 3.5$ in Figures 8c and 8d.

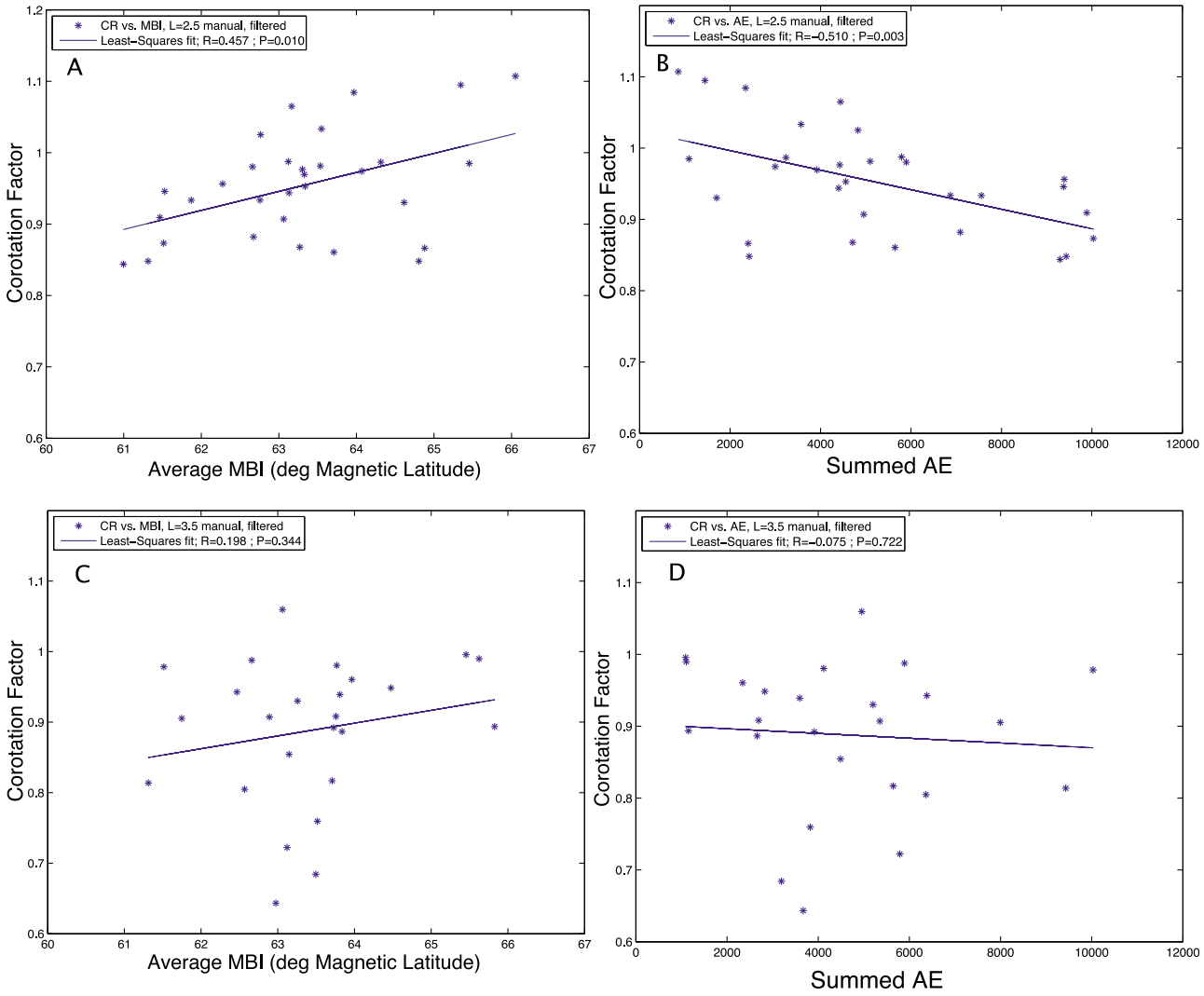

Figure 9. (a and c) Average MBI and (b and d) summed *AE* in the 24 h preceding the event plotted versus corotation factor, for filtered events only. Shown for $L = 2.5$ in Figures 9a and 9b and $L = 3.5$ in Figures 9c and 9d.

factors but high summed *Dst* and low summed *Kp* in the 24 h preceding the event. The ionospheric disturbance dynamo effect should appear as a correlation with the *AE* and MBI indices and the estimates of Joule heating from the AMIE model. Results in Figures 9 and 10 suggest that such a correlation also exists, again observed at $L = 2.5$ but not at $L = 3.5$.

[32] The existence of correlations only at the lower L-shell is surprising, as both ionospheric and magnetospheric influences on rotation rate would be expected to be stronger at higher L shells than at lower L shells, but most of our results imply the opposite. The dawn-dusk asymmetry effect should be important at higher L shells, where the corotation electric field is naturally weaker and the convection electric field has a stronger influence; and the ionospheric disturbance dynamo should have its strongest effect just equatorward of the auroral zone, which also corresponds to the outer parts of the plasmasphere. Yet our results show correlations at the lower L-shell and not at the higher one. One possibility is that the increased variability of convection electric fields at higher L shells could lead to more variation in corotation factor on finer timescales than at lower L, and thus less correlation with geomagnetic and auroral indices. If the influence on rotation rate by the magnetospheric and ionospheric mechanisms is as weak as suggested by the low correlation coefficients we observe at $L = 2.5$, perhaps the drift path behavior in the outer part of the plasmasphere is too dynamic due to variations in convection electric field and the variable position of the separatrix between open and closed drift paths, and any control that would be exerted by the disturbance dynamo is overwhelmed by other effects. Perhaps a simple azimuthal rotation rate observed in a circular annulus in the EUV image is inadequate in revealing the influence of geomagnetic and auroral activity on rotation, especially because any inaccuracy in the mapping of EUV radiance into the geomagnetic equator due to use of a simple dipole field would likely be higher at the higher L-shell, and the drift paths at $L = 3.5$ may not be completely circular around the Earth. It is also possible that we simply do not have enough reliable measurements of rotation rate at $L =$

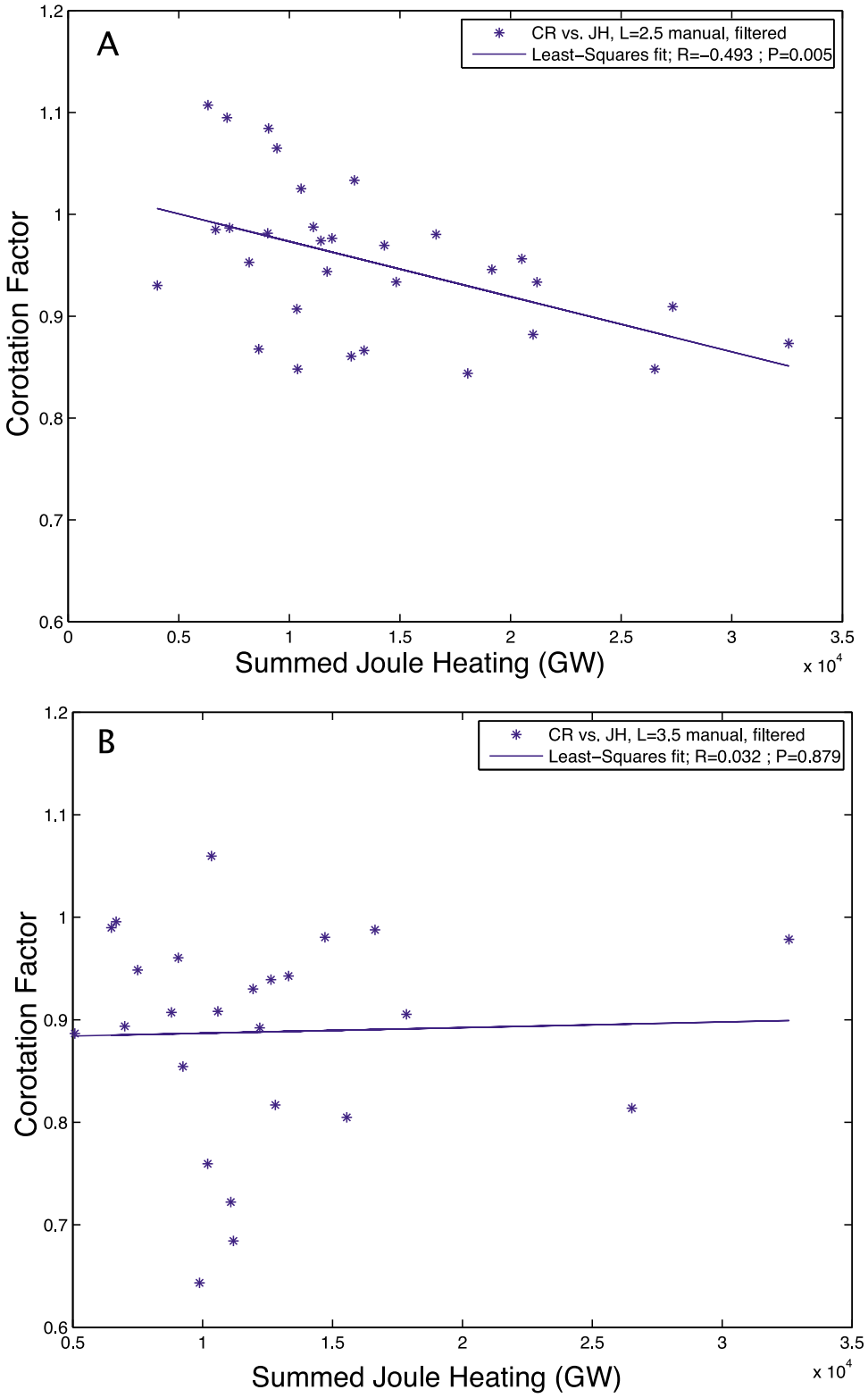

Figure 10. Summed Joule heating estimates in the 24 h preceding the event plotted versus corotation factor, for filtered events only. Shown for (a) L = 2.5 and (b) L = 3.5.

3.5, but given that the measurements do not hint at a correlation, we can currently draw no conclusions as to why these influences are not seen at higher L, and it remains an open question deserving further investigation.

[33] In the case of Figures 12 and 13, there does appear to be an L-shell effect on rotation rate, as the 18–21 MLT bin has a mean corotation factor of 0.87 at L = 2.5 (with quartile error bars at 0.71 and 1.02) and 0.76 at L = 3.5 (with quartile

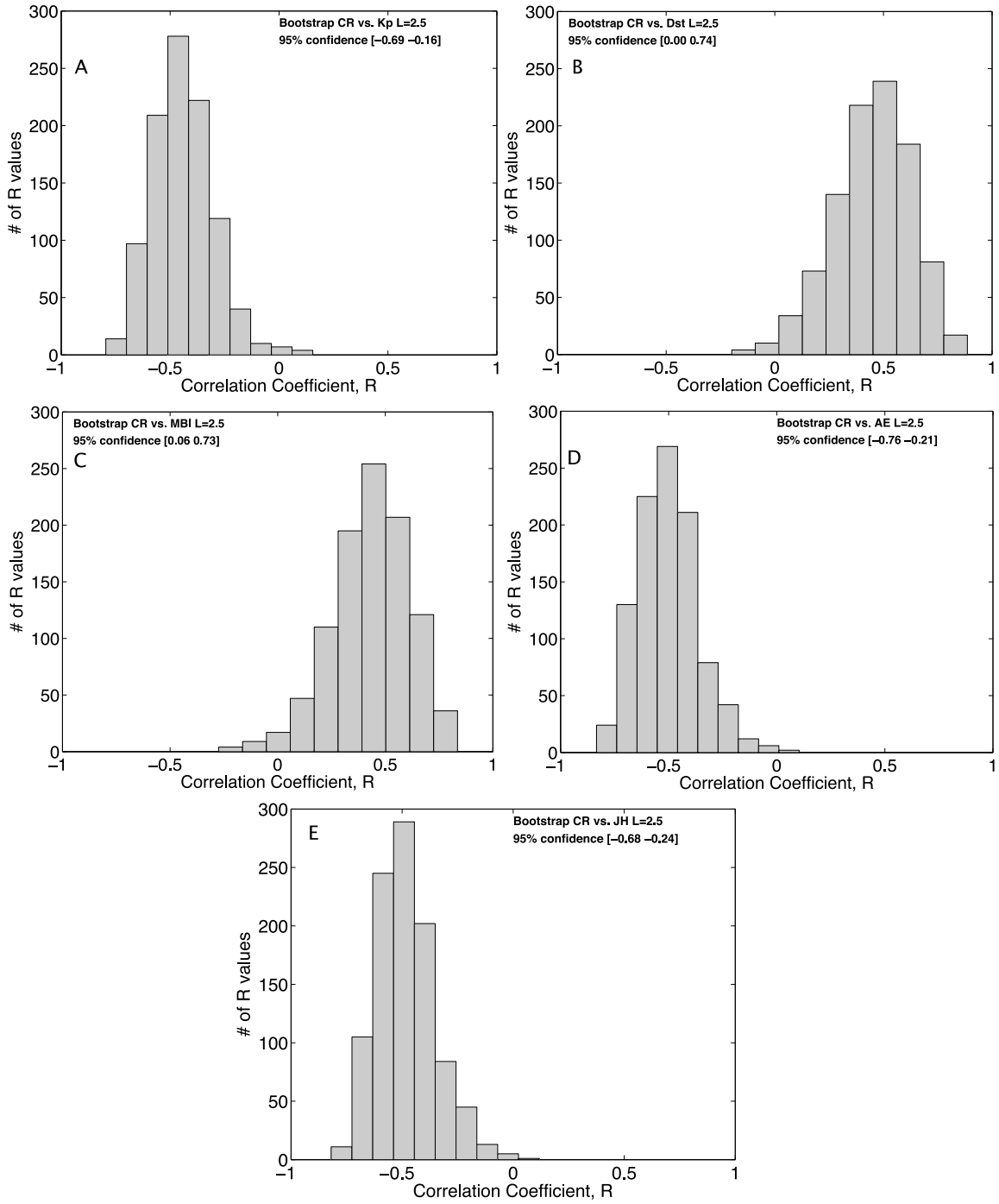

Figure 11. Bootstrapping analysis of correlation coefficients obtained between corotation factors and (a) *Kp*, (b) *Dst*, (c) MBI, (d) *AE*, and (e) Joule heating at $L = 2.5$.

error bars at 0.60 and 0.91). One would expect the rotation rate to be lower on the duskside compared with the dawnside, and that the rate would decrease at higher L shells, as implied by these results. Also, if the *Burch et al.* hypothesis is true, one might expect to see more storm-time subcorotation on the nightside of the Earth, as that is where much of the auroral precipitation and Joule heating occurs during a geomagnetic storm. Although we were unable to manually track features across midnight due to the Earth's shadow inhibiting our ability to distinguish azimuthal brightness features in that region, Figures 12 and 13 do show lower mean corotation factors in the evening and early morning sectors, as we might expect.

[34] Given that the MLT dependence of the rotation rate is superimposed upon other potential causes of subcorotation, it is possible that the dusk slowdown is partially obscuring a correlation between corotation factor and the auroral and geomagnetic indices. We attempted to account for this using two approaches: First, we filtered our corotation factors to exclude those events where the feature being tracked entered

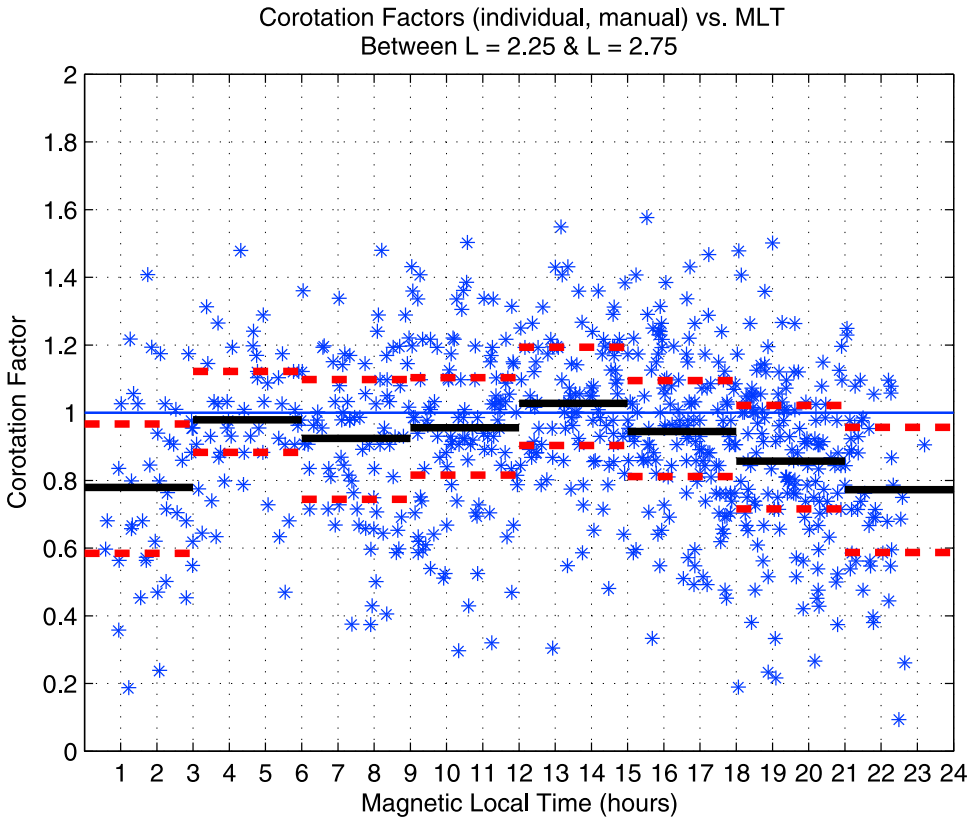

Figure 12. Manual corotation factors versus local time at $L = 2.5$. Short horizontal solid lines are means binned every 3 h. Dashed lines are the upper and lower quartile bars for those bins. Long horizontal line represents strict corotation.

into the dusk region (which we defined as MLT 16 to 24). Second, we used the binned mean corotation factor values displayed as the horizontal bars in Figures 12 and 13 to generate a "correction factor" that we then applied to the actual corotation factors for each event by dividing the measured corotation factor by the mean corotation factor for that local time bin. For instance, if a measured corotation factor for an event at $L = 2.5$ was 0.9 at an MLT of 19, when the binned mean corotation factor was 0.86, then the corrected corotation factor would be 0.9/0.86 = 1.05, because the measured factor was higher than the mean factor for that MLT.

[35] Having either limited or modified our measured corotation factors using the two methods described above, we then repeated our tests for correlation with each of the auroral and geomagnetic indices. In all cases, the corotation factors that were "corrected" according to the mean rotation rate at that local time resulted in lower correlation coefficients than the comparisons between the original corotation factors and the geomagnetic indices. Hence, the "correction factor" method did not succeed in revealing any hidden correlation between rotation rate and the indices. In some cases, the comparisons between the corotation factors from events outside of the 16–24 MLT range and the geomagnetic and auroral indices did yield slightly higher correlation coefficients than those in the non-MLT-limited comparisons shown in Figures 8–10. However, limiting the events used in this way reduced the number of usable events from 31 to 11 at $L = 2.5$ and from 25 to 6 at $L = 3.5$. Although these higher correlation coefficients for events that are not affected by the dusk slowdown in rotation rate do imply a real correlation between the auroral and geomagnetic indices and the plasmaspheric rotation rate, the small number of events used to produce those correlations leads us to base our conclusions more on the non-MLT-limited comparisons shown in Figures 8–10. When dusk slowdown effects are removed, a weak but significant correlation between rotation rate and geomagnetic activity, as well as between rotation rate and auroral energy input, remains. The dusk slowdown does not significantly obscure a correlation between measured corotation factor and auroral or geomagnetic index, and the measured corotation factors are probably a result of a superposition of auroral energy input, geomagnetic activity level, and local time.

[36] Finally, we note that, even in the filtered distributions, several events exhibit superrotation of the plasmasphere. For example, the event from 30 April 2001 22:35 UT to 1 May 2001 04:43 UT has a corotation factor of 1.11 as determined by both the automated cross-correlation routine and the manual feature tracking technique. The feature being tracked traversed magnetic local times 12.8–19.6 MLT. Also, the event ranging from 29 June 2001 18:11 UT to 30 June 02:23 UT has an automated corotation factor of 1.13 and a manual corotation factor of 1.09. The feature being tracked traversed 8.5–11.9 MLT. These events are visible as the two data points with the highest corotation factors in Figures 8–10 at $L = 2.5$. There are several other mea-

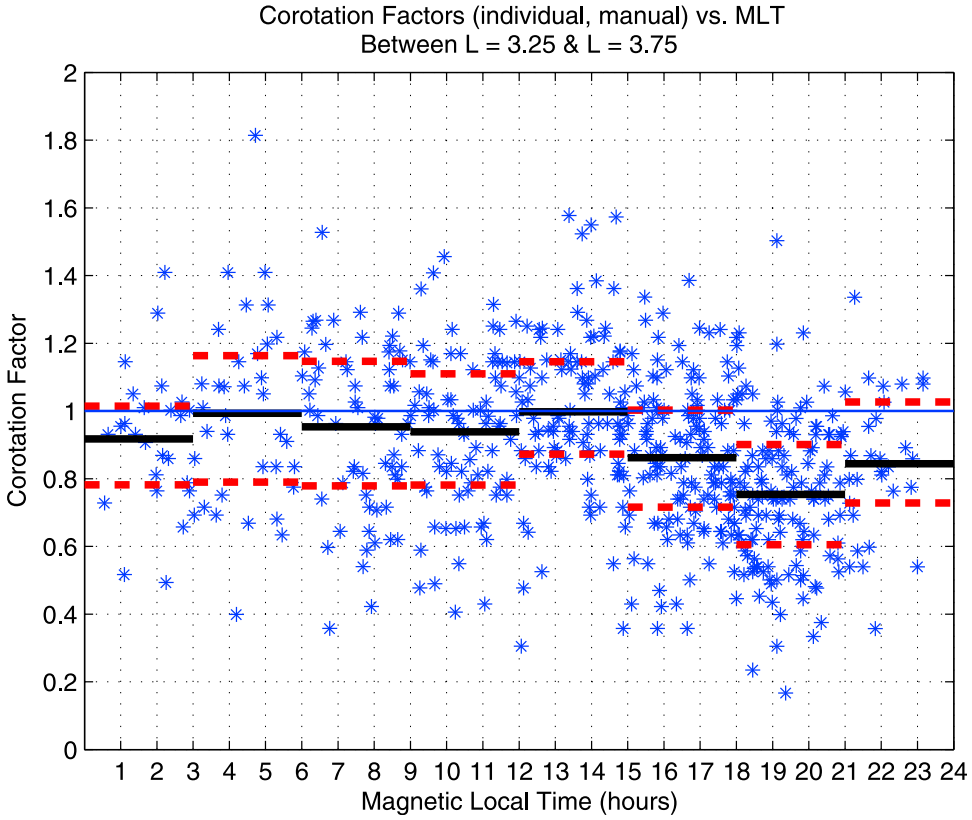

Figure 13. Manual corotation factors versus local time at $L = 3.5$. Short horizontal solid lines are means binned every 3 h. Dashed lines are the upper and lower quartile bars for those bins. Long horizontal line represents strict corotation.

surements of superrotation with even higher corotation factors than these in the full, unfiltered data set, but they are considered less reliable as the two different measurement techniques gave values differing by more than 0.05. We have checked ionospheric plasma drift measurements from the IDMs on the DMSP satellites for the same UT and MLT time ranges of these two events, as was done by *Gallagher et al.* [2005] and *Burch et al.* [2004], and find significant eastward ionospheric drift near magnetic latitude of 50 degrees, corresponding to $L = 2.5$. To our knowledge, these are the first known observations of plasmaspheric superrotation in EUV images, though such behavior in the upper atmosphere has been discussed by *Rishbeth* [1972].

5. Conclusions

[37] The variability of the plasmaspheric rotation rate observed by IMAGE EUV is likely due to a variety of causes. The accuracy and precision limitations of the measurements themselves, the evolution of the plasmasphere's morphology over the event time period, actual variability in the rotation rate depending on local time, geomagnetic and auroral activity all contribute to the variability in the corotation factor measurements obtained in this study. We have observed that, on average, the plasmasphere rotates at a mean corotation factor of 0.88–0.95, depending on L-shell. An analysis of up to 128 different corotation measurement events yields little indication of correlation between rotation rate and geomagnetic indices, but an analysis of a subset of corotation factors for which both an automated and a manual technique are in close agreement (within 0.05 of one another) does reveal a weak but significant correlation at $L = 2.5$. In general, for these higher-confidence measurements, lower corotation factors are associated with higher geomagnetic and auroral activity, and higher hemispheric Joule heating, and corotation and superrotation are associated with periods of lower activity. No significant correlation is observed at $L = 3.5$, which is surprising given one would expect a stronger influence at higher L due to both the disturbance dynamo and the dawn-dusk asymmetry. The *Burch et al.* [2004] hypothesis that the ionospheric disturbance dynamo is one cause of plasmasphere corotation lag is supported by our results of weak correlations with *AE*, MBI, and Joule heating, though the effect is apparently not strong enough to dominate the observed behavior, and is likely not the only phenomenon causing rotation rate variability. The storm-phase-dependent dawn-dusk asymmetry of electric potential provides another possible source of rotation variability, and is similarly supported based on weak correlations with summed *Kp* and *Dst*. The observed dependence of rotation rate on MLT shows that the plasmasphere rotates more slowly on the duskside than the dawnside, and that this effect is stronger at $L = 3.5$ than at $L = 2.5$, as expected. We also observe the first clear evidence of plasmaspheric superrotation. Our study makes clear that the rotation rate of the plasmasphere can be highly variable

and can differ greatly from perfect corotation, even at L shells as low as 2.5.

[38] **Acknowledgments.** This research was supported by a NASA Graduate Student Research Program (GSRP) fellowship (grant NNG05GL87H), a NASA Guest Investigator grant (NNG04GG43G), and a NSF grant (ATM-0348398). Work at the University of Arizona was supported by NASA grant NNX07AG46G. G.C. was supported by NSF grant ATM-0703335 from the GEM program. We thank Terry Forrester for his insightful comments and discussion regarding the EUV data itself as well as IDL EUV analysis tools available at http://euv.lpl.arizona.edu/euv/index.html.

[39] Zuyin Pu thanks Jerry Goldstein, Dennis Gallagher, and another reviewer for their assistance in evaluating this paper.

References

Baumjohann, W., and R. A. Treumann (1997), *Basic Space Plasma Physics*, Imperial College Press, London.

Berube, D., M. B. Moldwin, and M. Ahn (2006), Computing magnetospheric mass density from field line resonances in a realistic magnetic field geometry, *J. Geophys. Res.*, *111*, A08206, doi:10.1029/2005JA011450.

Bevington, P. R., and D. K. Robinson (2003), *Data Reduction and Error Analysis for the Physical Sciences*, McGraw-Hill, New York.

Blanc, M., and A. D. Richmond (1980), The ionospheric disturbance dynamo, *J. Geophys. Res.*, *85*, 1669–1686, doi:10.1029/JA085iA04p01669.

Brice, N. M. (1967), Bulk motion of the magnetosphere, *J. Geophys. Res.*, *72*, 5193–5211, doi:10.1029/JZ072i021p05193.

Brown, M. E. (1994), Observation of mass loading in the Io plasma torus, *Geophys. Res. Lett.*, *21*, 847–850, doi:10.1029/94GL00564.

Brown, R. A. (1983), Observed departure of the Io plasma torus from rigid corotation with Jupiter, *Astrophys. J.*, *268*, L47–L50, doi:10.1086/184027.

Burch, J. L., J. Goldstein, and B. R. Sandel (2004), Cause of plasmasphere corotation lag, *Geophys. Res. Lett.*, *31*, L05802, doi:10.1029/2003GL019164.

Darrouzet, F., et al. (2008), Plasmaspheric density structures and dynamics: Properties observed by the CLUSTER and IMAGE missions, *Space Sci. Rev.*, *168*, 55–106, doi:10.1007/s11214-008-9438-9.

Davis, T. N., and M. Sugiura (1966), Auroral electrojet activity index *AE* and its universal time variations, *J. Geophys. Res.*, *71*, 785–801.

Gallagher, D. L., M. L. Adrian, and M. W. Liemohn (2005), Origin and evolution of deep plasmaspheric notches, *J. Geophys. Res.*, *110*, A09201, doi:10.1029/2004JA010906.

Galvan, D. A., M. B. Moldwin, and B. R. Sandel (2008), Diurnal variation in plasmaspheric He^+ inferred from extreme ultraviolet images, *J. Geophys. Res.*, *113*, A09216, doi:10.1029/2007JA013013.

Gold, T. (1968), Rotating neutron stars as the origin of the pulsating radio sources, *Nature*, *218*, 731–732, doi:10.1038/218731a0.

Goldstein, J., B. R. Sandel, M. F. Thomsen, M. Spasojeviæ, and P. H. Reiff (2004), Simultaneous remote sensing and in situ observations of plasmaspheric drainage plumes, *J. Geophys. Res.*, *109*, A03202, doi:10.1029/2003JA010281.

Gussenhoven, M. S., D. A. Hardy, and W. J. Burke (1981), DMSP/F2 electron observations of equatorward auroral boundaries and their relationship to magnetospheric electric fields, *J. Geophys. Res.*, *86*, 768–778, doi:10.1029/JA086iA02p00768.

Hill, T. W. (1979), Inertial limit on corotation, *J. Geophys. Res.*, *84*, 6554–6558, doi:10.1029/JA084iA11p06554.

Kelley, M. C. (2009), *The Earth's Ionosphere: Plasma Physics and Electrodynamics*, *Int. Geophys. Ser.*, vol. 96, Elsevier, San Diego, Calif.

Kronberg, E. A., K.-H. Glassmeier, J. Woch, N. Krupp, A. Lagg, and M. K. Dougherty (2007), A possible intrinsic mechanism for the quasi-periodic dynamics of the Jovian magnetosphere, *J. Geophys. Res.*, *112*, A05203, doi:10.1029/2006JA011994.

Liemohn, M. W., A. J. Ridley, D. L. Gallagher, D. M. Ober, and J. U. Kozyra (2004), Dependence of plasmaspheric morphology on the electric field description during the recovery phase of the 17 April 2002 magnetic storm, *J. Geophys. Res.*, *109*, A03209, doi:10.1029/2003JA010304.

Lu, G., P. H. Reiff, M. R. Hairston, R. A. Heelis, and J. L. Karty (1989), Distribution of convection potential around the polar cap boundary as a function of the interplanetary magnetic field, *J. Geophys. Res.*, *94*, 13,447–13,461, doi:10.1029/JA094iA10p13447.

Lu, G., A. D. Richmond, J. M. Ruohoniemi, R. A. Greenwald, M. Hairston, F. J. Rich, and D. S. Evans (2001), An investigation of the influence of data and model inputs on assimilative mapping of ionospheric electrodynamics, *J. Geophys. Res.*, *106*, 417–434, doi:10.1029/2000JA000606.

Mozer, F. S. (1970), Electric field mapping in the ionosphere at the equatorial plane, *Planet. Space Sci.*, *18*, 259–263, doi:10.1016/0032-0633(70)90161-3.

Mozer, F. S. (1973), Electric fields and plasma convection in the plasmasphere, *Rev. Geophys.*, *11*, 755–765, doi:10.1029/RG011i003p00755.

Nishida, A. (1966), Formation of plasmapause, or magnetospheric plasma knee, by the combined action of magnetospheric convection and plasma escape from the tail, *J. Geophys. Res.*, *71*, 5669–5679.

Pontius, D. H., Jr., and T. W. Hill (1982), Departure from corotation of the Io plasma torus: Local plasma production, *Geophys. Res. Lett.*, *9*, 1321–1324, doi:10.1029/GL009i012p01321.

Reiff, P. H. (1990), The use and misuse of statistics in space physics, *J. Geomagn. Geoelectr.*, *42*, 1145–1174.

Ridley, A., T. Gombosi, and D. Dezeeuw (2004), Ionospheric control of the magnetosphere: Conductance, *Ann. Geophys.*, *22*, 567–584.

Rishbeth, H. (1972), Superrotation of the upper atmosphere, *Rev. Geophys.*, *10*, 799–819, doi:10.1029/RG010i003p00799.

Roelof, E. C., and A. J. Skinner (2000), Extraction of ion distributions from magnetospheric ENA and EUV images, *Space Sci. Rev.*, *91*, 437–459, doi:10.1023/A:1005281424449.

Romanova, M. M., G. V. Ustyugova, A. V. Koldoba, and R. V. E. Lovelace (2002), Magnetohydrodynamic simulations of disk-magnetized star interactions in the quiescent regime: Funnel flows and angular momentum transport, *Astrophys. J.*, *578*, 420–438, doi:10.1086/342464.

Sandel, B. R., et al. (2000), The extreme ultraviolet imager investigation for the IMAGE mission, *Space Sci. Rev.*, *91*, 197–242, doi:10.1023/A:1005263510820.

Sandel, B. R., J. Goldstein, D. L. Gallagher, and M. Spasojevic (2003), Extreme ultraviolet imager observations of the structure and dynamics of the plasmasphere, *Space Sci. Rev.*, *109*, 25–46, doi:10.1023/B:SPAC.0000007511.47727.5b.

Senior, C., and M. Blanc (1984), On the control of magnetospheric convection by the spatial distribution of ionospheric conductivities, *J. Geophys. Res.*, *89*, 261–284, doi:10.1029/JA089iA01p00261.

Slavin, J. A., et al. (2008), Mercury's magnetosphere after MESSENGER's first flyby, *Science*, *321*, 85–89, doi:10.1126/science.1159040.

Spasojević, M., J. Goldstein, D. L. Carpenter, U. S. Inan, B. R. Sandel, M. B. Moldwin, and B. W. Reinisch (2003), Global response of the plasmasphere to a geomagnetic disturbance, *J. Geophys. Res.*, *108*(A9), 1340, doi:10.1029/2003JA009987.

Tokar, R. L., et al. (2006), The interaction of the atmosphere of Enceladus with Saturn's plasma, *Science*, *311*, 1409–1412, doi:10.1126/science.1121061.

G. Crowley, Atmospheric and Space Technology Research Associates, 12703 Spectrum Dr., Ste. 101, San Antonio, TX 78249, USA.

D. A. Galvan, Jet Propulsion Laboratory, California Institute of Technology, 4800 Oak Grove Dr., M/S 138-308, Pasadena, CA 91109, USA. (david.galvan@jpl.nasa.gov)

M. B. Moldwin, Department of Atmospheric, Oceanic and Space Sciences, University of Michigan, 2455 Hayward St., Ann Arbor, MI 48109-2143, USA.

B. R. Sandel, Lunar and Planetary Laboratory, University of Arizona, Sonett Space Sciences Bldg., 1541 East University Blvd., Tucson, AZ 85721-0063, USA.